Study on Arrangement of Diblock Copolymer Microdomains during Solvent Evaporation and in Hemi-spherically Confined System

Myung-Hyun Kim

Department of Materials Science Engineering

Graduate school of UNIST

2014

Study on Arrangement of Diblock Copolymer Microdomains during Solvent Evaporation and in Hemi-spherically Confined System

Myung-Hyun Kim

Department of Materials Science Engineering

Graduate school of UNIST

Study on Arrangement of Diblock Copolymer Microdomains during Solvent Evaporation and in Hemi-spherically Confined System

A thesis

submitted to the Graduate School of UNIST

In partial fulfillment of the

requirements for the degree of

Master of Science

Myung-Hyun Kim

06.20.2014

_____

Major Advisor

Jaeup Kim

Study on Arrangement of Diblock Copolymer Microdomains during Solvent Evaporation and in Hemi-spherically Confined System

Myung-Hyun Kim

This certifies that the thesis of Myung-Hyun Kim is approved.

06.20.2014

signature

_____

Thesis Supervisor: Jaeup Kim

signature

_____

Myoung Hoon Song: Thesis Committee Member # 1

signature

_____

Jung-Woo Yoo: Thesis Committee Member #2

ABSTRACT

Block copolymer nanostructures are one of the cutting edge candidates to create long range ordered microstructures. *AB* block copolymers can be assembled into various nanoscale morphologies such as lamella, cylinder, sphere and gyroid depending on the *A* block composition *f* and the interaction strength between segments represented by the Flory-Huggins χ parameter. There have been intense efforts to use the block copolymer morphologies as scaffolds to position nanomaterials into ordered arrays for applications such as high density memory device, metamaterial, and photonic band gap materials. Solvent evaporation and annealing is one of the most common methods to create the block copolymer structure in thin films and enhance its alignment. However, the microdomains usually contain some uncontrolled defects and lack of long-range order due to entropic fluctuation and incomplete annealing. The optimum structural property required in the academic and industrial world can be outlined by the following three keywords: Large area, low defects, and short period. The detailed discussion for these three trendy keywords in this rapidly growing field is included in chapter I.

In chapter II, I introduce the main theoretical tool in this research, self-consistent field theory (SCFT), and its application. The most important part in SCFT method is the calculation of partition function which predicts statistical behavior of polymers by solving the modified diffusion equation with potential field $w(\mathbf{r})$. The commonly used numerical methods to solve such equations are real space method, spectral method and pseudospectral method. In this study, I use the real space method to investigate the microstructure evolution of the diblock copolymer thin films in solvent. I also use the pseudospectral method to obtain the morphology of the block copolymers formed in the confined system with two controlled interfaces.

In the third chapter, I study the nanostructure evolution of diblock copolymer thin films in solvents. I use SCFT to study the equilibrium block copolymer phases and the quasi-equilibrium dynamic path of the morphology evolution during the slightly selective solvent vaporization process. During the evaporation process, I introduce a small noise field using random function to create the initial block copolymer morphologies. Then, the thickness of block copolymer film *h* is reduced as the global solvents volume fraction ψ decreases. During this process, I use the previous morphologies as an input for the morphology of the thinner film, which means I model the quasi-static morphology evolution of the thin film. As the solvent evaporates, the film thickness decreases and the number of defects also decrease. This method allows us to track down the detailed mechanism of the defect elimination. The onset of order-disorder transition and the observed morphology matches very well with the theoretical prediction.

Confinement of diblock copolymers under certain geometries can offer new methods to develop unique morphologies which have never been known before in bulk or thin film. In chapter IV, I study various block copolymer morphologies in hemispherical and ellipsoidal shape confinements and compare the results with experiments. In the experiment, PS-PMMA block copolymers are physically confined in hemispherical cavities prepared by anodic aluminum oxide template. The cavities have two controlled interfaces, one of them is the top surface of the cavity covered with preferential films and the other is the surface of cavity wall which interacts preferentially or randomly depending on the coating of the cavity wall. Our theoretical modeling uses SCFT which calculates the mean field density distribution of AB block copolymers in this confined geometry. The key parameters for the morphology determination are the size and shape of the container and the surface tension between components. For example, when the container wall is coated with PS polymers and neutral cover film is used, onion-shape lamellar phases with PS at the bottom is observed rather than the parallel lamellar phases. It is also found that preferential cover film promotes the alignment of domains. Our versatile method also allows us to model ellipsoid-shaped confinements, and other interesting morphologies are found depending on the eccentricity of the ellipsoid.

Contents

LIST OF FIGURES

I. Significance of the study

1.1. Introduction

In recent decades, the development of polymers with a new molecular structure and functions has great impacts on the development of modern science and technology producing a tremendous amount of research results. Among them, the research of block copolymers (BCPs) has received great attention as a useful tool for the development of nanotechnology[1-4].

A polymer refers to a macromolecule which consists of repeating units called monomers. If the polymer is produced from one type of monomers, the product material is called homopolymers. If two or more types of monomers are used, the product material becomes a copolymer. In the copolymer, monomers can be randomly aligned (random copolymers), crossed (alternating copolymers) or aligned in block (block copolymers, see Figure 1a).
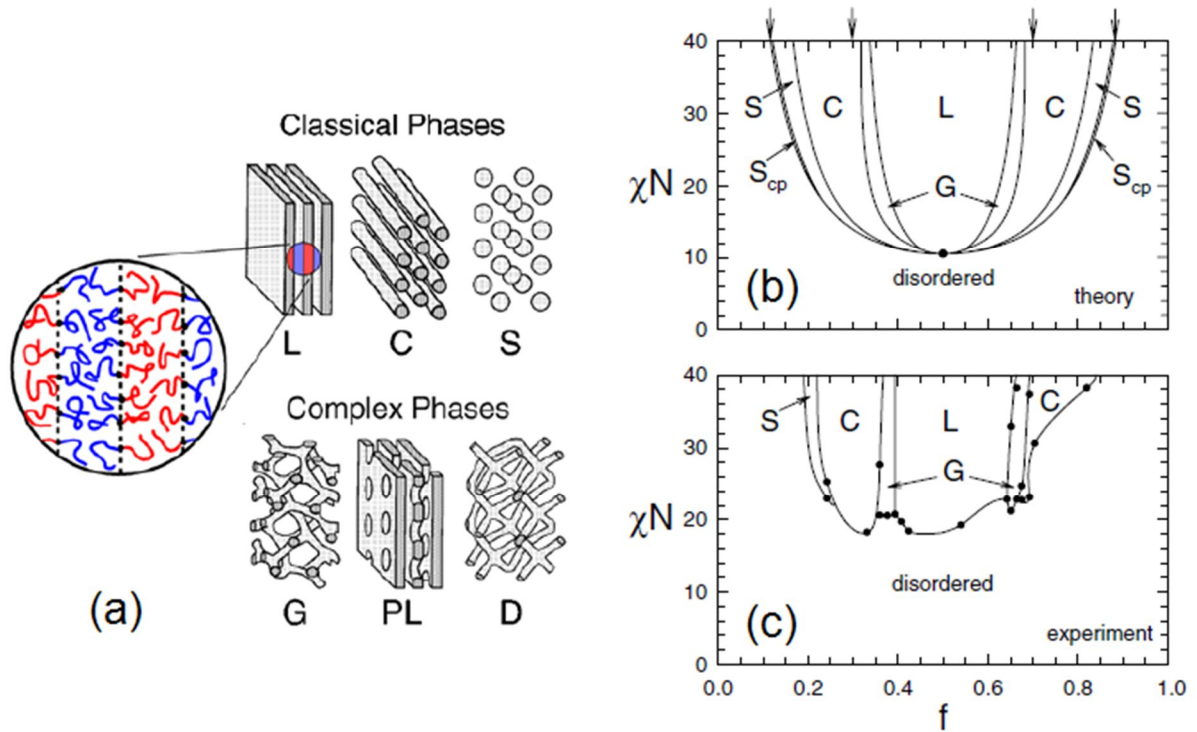
Figure 1. (a) Various *AB* block copolymer phases. (b) The equilibrium phase diagram predicted by SCFT theory. (c) The equilibrium phase diagram obtained from experiment.

Especially, a diblock copolymer is a linear chain with two different homopolymers connected by a

covalence bond, and their properties are affected by the composition f between blocks constituting the block copolymer, chain length N, Flory-Huggins interaction parameter χ. BCPs with large χN are known to phase separate due to the repulsion between different blocks. However, since they are connected by the covalence bond, the degree of the phase separation is limited so that they assemble into simple nanostructures with periodic alignments such as lamella, cylinder and sphere or complex nanostructures with three dimensional networks such as gyroid or perforated lamella. The nanostructures created in this way can be adjusted up to the size of 5-100nm[5] (see Figure 1b). Because of this property, studies are actively carried out on their applications such as large-scale memory devices or optical bandgap materials which require periodic nanostructures.[6]

Currently, one of the wide fields of research is a method to precisely control the molecular structure of a nonstructured material using a block copolymer. In particular, the development of research on block copolymer incorporated into existing lithography technology, the core technology of the semiconductor industry, one of the big axes of modern industry shows a significant achievement.[7-8] Moreover, since the domain size of nanostructure formed by the self-assembly phenomenon of the block copolymer can be widely adjusted to 5-100nm, various forms of nano structure production are possible so it is expected that it will be applied to various next generation nano devices such as large-scale magnetic storage device,[9] nano wire production,[10-11] quantum dot[12-13] and metal dot.[14]

However, these studies on the block copolymer have some problems. First, it cannot get a nanostructure with a short period. For the next generation microchip technology, a nanostructure with a small period of less than 10nm is necessary, but with simple adjustment of molecular amount, phase separation may not occur. Thus, to make this short period, recently, experimental efforts are active to develop a new material of block copolymer with great χ and small N.[15]
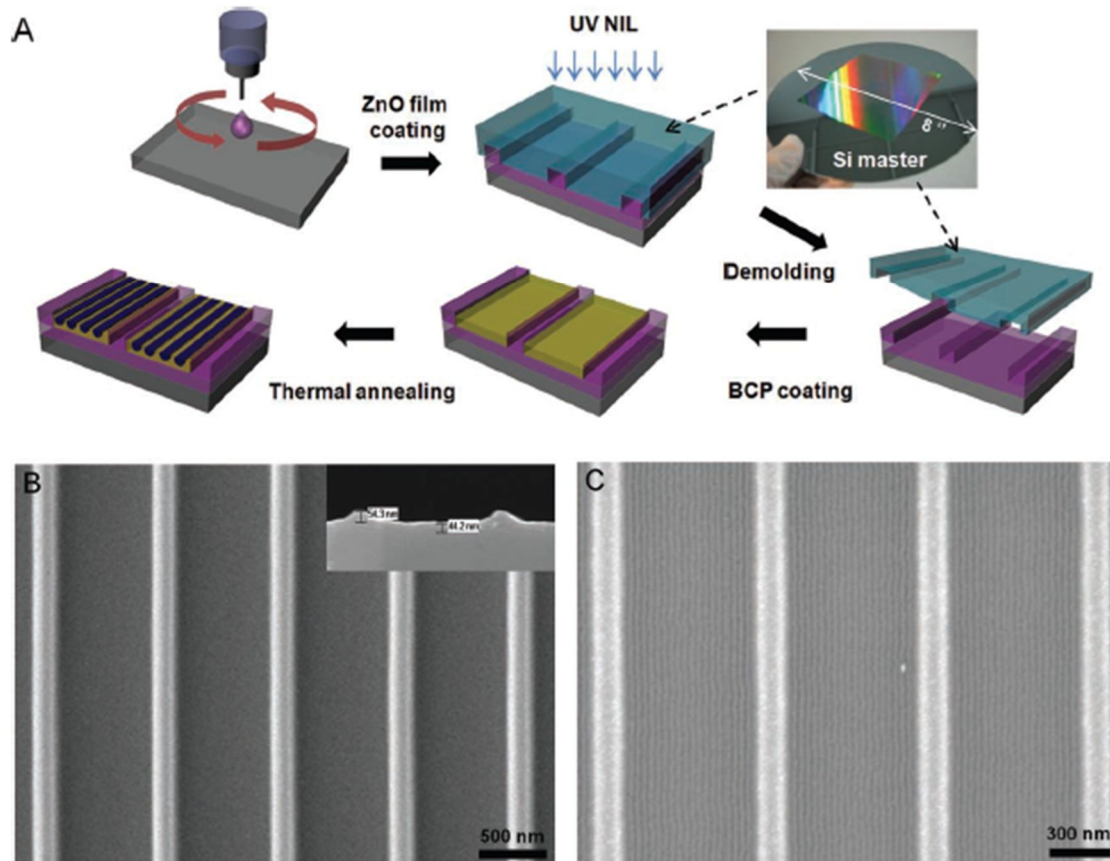
Figure 2. (A) Direction controlled self-assembly strategy of PS-b-PMMA film on Zinc oxide pattern. (B) Zinc oxide pattern. (C) Aligned cylindrical array (SEM image). (Figure 2b,c of Ref. [53])

Second, it is difficult to get defect-free or low-defect pattern. In order to be applied to the real industry, the domain of the nanometer size needs a structure repeated to macro size without defects, but it is not easy to make a nanostructure such a defect-free macro size in a system of thermodynamic self-assembly. To reduce structure defects and produce various patterns, various methods are used: e.g. third-dimensional lamination on the two-dimensional pattern or repeated lamination through optic lithography or lamination by repeated imprinting/transference (See, Figure 2). In the meantime, solvent evaporation and annealing are most common methods to make BCPs nanostructure, but these methods are usually accompanied by uncontrolled defects. Entropic fluctuation seems to be the cause, but in order to control the formation of defects and remove the defects completely, it is necessary to understand the evaporation mechanism between BCPs and solution carried out in real time.

Thirdly, the size of BCPs in periodic domain that can be obtained from the laboratory currently is about hundreds of nm, from an academic point of view, it is enough for the purpose of the study, but for practical application, an area with micro square meters or larger is necessary. Thus, for a study of the theory of large-area BCPs, recently developed new algorithms should actively be introduced, and it is necessary to develop an efficient algorithm using parallel calculation like OpenMP (Open Multi-Processing) or MPI (Massage Passing Interface) to increase computation efficiency.

In summary, nanotechnology is recognized as one of the core technologies in the future. Among them, our focus is on the alignment of wide area of nanostructure with novel electric, optical or magnetic properties in the scale of approximately 10 nm or less[16-19], which could initiate the innovation of energy and information technology. I expect my research on the theory of diblock copolymers can contribute to the development of new nanomaterials and their application to industrial world.

II. Introduction of self-consistent field method and its application

2.1. Self-Consistent Field Theory

For the study of the block copolymer, the basic background theory used in this project is SCFT. This method begins from the calculation of the partial partition function which predicts the statistical behavior of polymer materials. An *AB* block copolymer is modeled as a flexible Gaussian chain composed of *N* segments with statistical segment length *a*. The partition function $q(\mathbf{r},s)$ representing the existence probability of the polymer fragment with a length *sN* starting from the *A* end can be calculated by solving the following modified diffusion equation

$$\frac{\partial}{\partial s}q(\mathbf{r},s) = \left[\frac{a^2 N}{6}\nabla^2 - w(\mathbf{r})\right]q(\mathbf{r},s) \qquad (1)$$

$$-\frac{\partial}{\partial s}q^\dagger(\mathbf{r},s) = \left[\frac{a^2 N}{6}\nabla^2 - w(\mathbf{r})\right]q^\dagger(\mathbf{r},s) \qquad (2)$$

where $w(\mathbf{r})$ is a self-consistent mean field acting on the polymers. If the *A* block ratio is *f*, the field $w_A(\mathbf{r})$ acting on polymer *A* is used when $s < f$, and the field $w_B(\mathbf{r})$ acting on polymer *B* is used

when $s > f$. For the case of diblock copolymer melts, the equations determining the two fields are the following self-consistency equations:

$$w_A(\mathbf{r}) = \xi(\mathbf{r}) + \chi N \phi_B(\mathbf{r}) \qquad (3)$$

$$w_B(\mathbf{r}) = \xi(\mathbf{r}) + \chi N \phi_A(\mathbf{r}) \qquad (4)$$

where $\xi(\mathbf{r})$ is the pressure function enforcing the incompressibility of polymer melt, $\phi_i(\mathbf{r})$ is the segment density of i type polymers (A or B). Also, the partition function of one whole chain is given as the following formula:

$$Q = \int d\mathbf{r}\, q(\mathbf{r},s)\, q^\dagger(\mathbf{r},s) \qquad (5)$$

For a free polymer with no fixed end, the initial condition is $q(\mathbf{r},s) = 1$. The partial partition function $q^\dagger(\mathbf{r},s)$ of the polymer segments with a length $(1-s)N$ starting from the B end is calculated by solving the equation (2) subject to the initial condition $q^\dagger(\mathbf{r},s) = 1$.

Using the given value of the mean field $w(\mathbf{r})$, these differential equations are solved by numerical analysis in the initial condition, $q(\mathbf{r},0) = q^\dagger(\mathbf{r},1) = 1$, and then using the obtained partition functions, the density function of each polymer can be calculated as follows:

$$\phi_A(\mathbf{r}) = \frac{V}{Q} \int_0^{f_A} ds\, q(\mathbf{r},s)\, q^\dagger(\mathbf{r},s) \qquad (6)$$

$$\phi_B(\mathbf{r}) = \frac{V}{Q} \int_{f_A}^1 ds\, q(\mathbf{r},s)\, q^\dagger(\mathbf{r},s) \qquad (7)$$

To calculate the partition function by solving equation (1), field $w(\mathbf{r})$ is necessary, but this field can only be calculated using equations (6-7) after calculating the partition function. It is impossible to find the solution at a time avoiding this structure of circulation, so using iteration, the field with self-consistency with agreed input and output should be found. In other words, if the test input field is put in initially, the partition function is calculated, and from the polymer density calculated with that, the output field comes out, and from this information, a new input field is made, which modified the

5

original input field to try it in the next iteration step. Finally, after the field with self-consistency is obtained, free energy of each polymer in the calculation is expressed as follows:

$$\frac{F}{nk_BT} = -\ln\frac{Q}{V} + \frac{1}{V}\int d\mathbf{r}\left(\chi N\phi_A(\mathbf{r})\phi_B(\mathbf{r}) - w_A(\mathbf{r})\phi_A(\mathbf{r}) - w_B(\mathbf{r})\phi_B(\mathbf{r})\right) \qquad (8)$$

To go through the main points again, the strategy of SCFT is composed of four big steps.

① The starting point of this method is assuming an initial random field, because we do not know the true field until the last step.

② With this, we solve the modified diffusion equations for the two partial partition functions.

③ Next, we calculate the polymer concentration from partition function.

④ And then, we obtain the output fields from the concentrations. By comparing the input and output fields we use simple mixing method to create a new input field, if there exist some difference. Go back to step ① and continue iterations until the field equations and the incompressibility equation $(f_A + f_B = 1)$ are self-consistently satisfied.

If all these iterations are completed, we can obtain final free energy per one chain by equation (8). The exact mean-field polymer configuration and its energy is now obtained. This algorithm process is explained in the below Figure 3 (In this Figure, the unit length is set to be $a^2N = 1$).

$$q(\mathbf{r}, s)$$

Find partition function

$$\phi_A(\mathbf{r}) = \frac{V}{Q} \int_0^{f_A} ds\, q(\mathbf{r}, s)\, q^\dagger(\mathbf{r}, s)$$

$$\phi_B(\mathbf{r}) = \frac{V}{Q} \int_{f_A}^1 ds\, q(\mathbf{r}, s)\, q^\dagger(\mathbf{r}, s)$$

$$Q = \int d\mathbf{r}\, q(\mathbf{r}, s)\, q^\dagger(\mathbf{r}, s)$$

$$w_{\text{in}}(\mathbf{r})$$

Set input field (first randomly)

$$\phi(\mathbf{r})$$

Find each density

$$w_{\text{out}}(\mathbf{r})$$

Find output field

$$w_{\text{in}}^{\text{new}} = \lambda w_{\text{in}} + (1-\lambda) w_{\text{out}}$$
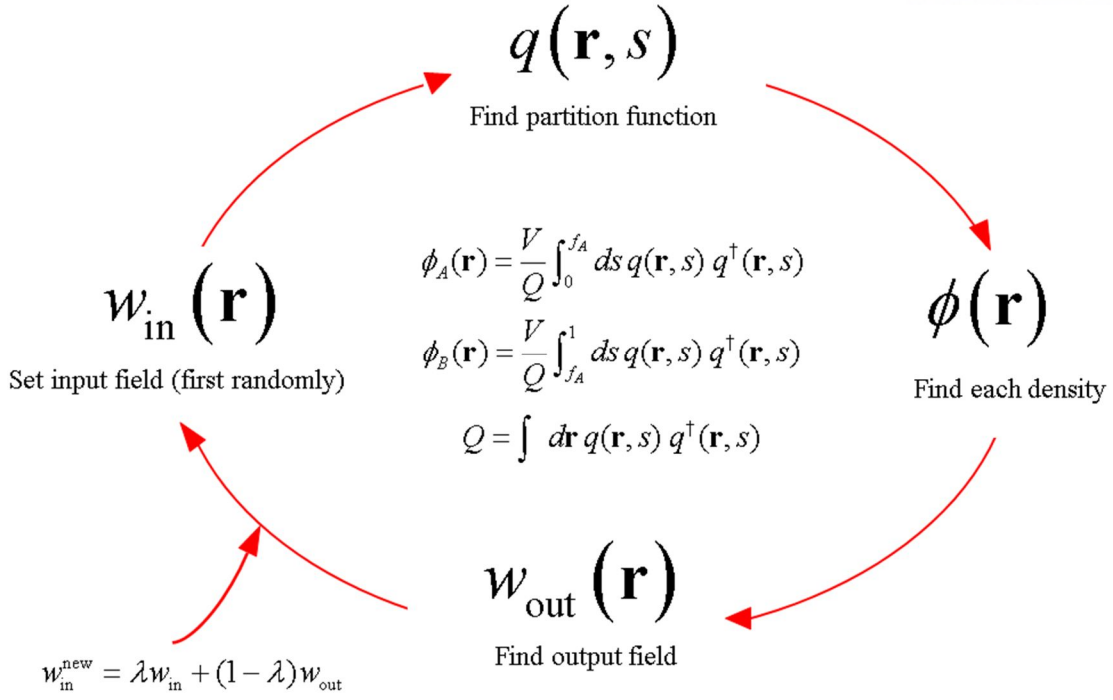
Figure 3. Iteration mechanism of SCFT.

The most core part in SCFT calculation is the very solution of the modified diffusion equations (1) and (2). Commonly used methods to solve them can be classified into real space method,[20-24] spectral method[25-27] and pseudospectral method,[28-31] and this study use the real space method to calculate the behavior of the polymer pattern in thin films, and using the pseudospectral method, the morphology of the block copolymer formed in the trapped system was calculated.

2.2.   Real Space Method

The SCFT real space method basically solves the above modified diffusion equation (1) using the finite difference method, and this study use Douglas-Gunn Algorithm which is known to be efficient in reducing errors of the finite difference method. Its starting point is to write down the three dimensional finite difference equation using the Crank-Nicolson method:

$$\frac{q_{ijk}^{n+1} - q_{ijk}^n}{\Delta s} = \left(\frac{1}{6} \left(\delta_x^2 + \delta_y^2 + \delta_z^2 \right) - w(i\Delta x, j\Delta y, k\Delta z) \right) \left(\frac{q_{ijk}^{n+1} + q_{ijk}^n}{2} \right) \tag{9}$$

where δ_x^2, δ_y^2, δ_z^2 are the quadratic differential operators in each direction, Δs is the step size in s

7

direction.

In the Douglas-Gunn Algorithm, this single equation is modified by the following three equations:

$$\frac{q_{ijk}^{*} - q_{ijk}^{n}}{\Delta s} = \frac{\delta_x^2}{12}\left(q_{ijk}^{*} + q_{ijk}^{n}\right) + \frac{\delta_y^2}{12}\left(q_{ijk}^{n} + q_{ijk}^{n}\right) + \frac{\delta_z^2}{12}\left(q_{ijk}^{n} + q_{ijk}^{n}\right) - \frac{w_{ijk}}{\Delta s}\left(q_{ijk}^{*} + q_{ijk}^{n}\right) \tag{10}$$

$$\frac{q_{ijk}^{**} - q_{ijk}^{n}}{\Delta s} = \frac{\delta_x^2}{12}\left(q_{ijk}^{*} + q_{ijk}^{n}\right) + \frac{\delta_y^2}{12}\left(q_{ijk}^{**} + q_{ijk}^{n}\right) + \frac{\delta_z^2}{12}\left(q_{ijk}^{n} + q_{ijk}^{n}\right) - \frac{w_{ijk}}{\Delta s}\left(q_{ijk}^{**} + q_{ijk}^{n}\right) \tag{11}$$

$$\frac{q_{ijk}^{n+1} - q_{ijk}^{n}}{\Delta s} = \frac{\delta_x^2}{12}\left(q_{ijk}^{*} + q_{ijk}^{n}\right) + \frac{\delta_y^2}{12}\left(q_{ijk}^{**} + q_{ijk}^{n}\right) + \frac{\delta_z^2}{12}\left(q_{ijk}^{n+1} + q_{ijk}^{n}\right) - \frac{w_{ijk}}{\Delta s}\left(q_{ijk}^{n+1} + q_{ijk}^{n}\right) \tag{12}$$

where

$$w_{ijk} \equiv \frac{\Delta s}{2} w(i\Delta x, j\Delta y, k\Delta z) \tag{13}$$

The advantage of this method is that the above three equations can be transformed to the following three equations which have the proper shape to apply the alternate-direction-implicit (ADI) technique,

$$\left(1 - \frac{\Delta s \delta_x^2}{12} + w_{ijk}\right)q_{ijk}^{*} = \left(1 + \frac{\Delta s \delta_x^2}{12} + \frac{\Delta s \delta_y^2}{6} + \frac{\Delta s \delta_z^2}{6} - w_{ijk}\right)q_{ijk}^{n} \tag{14}$$

$$\left(1 - \frac{\Delta s \delta_y^2}{12} + w_{ijk}\right)q_{ijk}^{**} = \left(1 + w_{ijk}\right)q_{ijk}^{*} - \frac{\Delta s \delta_y^2}{12}q_{ijk}^{n} \tag{15}$$

$$\left(1 - \frac{\Delta s \delta_z^2}{12} + w_{ijk}\right)q_{ijk}^{n+1} = \left(1 + w_{ijk}\right)q_{ijk}^{**} - \frac{\Delta s \delta_z^2}{12}q_{ijk}^{n} \tag{16}$$

i.e. when the three-point finite difference equations are used, one explicit calculation and one implicit calculation are carried out in every step, and the matrix equation appearing for the calculation utilizes a tridiagonal matrix. Suppose that M space grids and N polymer backbone grids are used, the number of operations necessary for one full partition function calculation is $\mathrm{O}(MN)$.

2.3.   Pseudospectral Method

In the SCFT pseudospectral method, the following diffusion equation should be solved.

$$\frac{\partial}{\partial s}q(\mathbf{r},s)=\left[\frac{1}{6}\nabla^2-w(\mathbf{r})\right]q(\mathbf{r},s)\equiv A\,q(\mathbf{r},s) \qquad (17)$$

A is an operator, which satisfies the following equation.

$$q(\mathbf{r},s)=e^{As}q(\mathbf{r},0) \quad\rightarrow\quad q(\mathbf{r},s+\Delta s)=e^{A\Delta s}q(\mathbf{r},s) \qquad (18)$$

Suppose that Δs calculation is carried out to time scale s, finally the following diffusion equation can be obtained.

$$q(\mathbf{r},s+\Delta s)=\exp\left[\frac{\Delta s}{6}\nabla^2-\Delta s w(\mathbf{r})\right]q(\mathbf{r},s) \qquad (19)$$

When the above equation is solved, in order to reduce errors, we can rewrite the equation symmetrically, and this method is called Strang Splitting.[33-34]

$$q(\mathbf{r},s+\Delta s)\cong\exp\left[\frac{-\Delta s w(\mathbf{r})}{2}\right]\exp\left[\frac{\Delta s}{6}\nabla^2\right]\exp\left[\frac{-\Delta s w(\mathbf{r})}{2}\right]q(\mathbf{r},s) \qquad (20)$$

To calculate this obtained equation, the differential equation is calculated through the following three steps.

$$q^{**}(\mathbf{r})=\exp\left[\frac{\Delta s}{6}\nabla^2\right]q^{*}(\mathbf{r}) \qquad (21)$$

$$q^{*}(\mathbf{r})=\exp\left[\frac{-\Delta s w(\mathbf{r})}{2}\right]q(\mathbf{r},s) \qquad (22)$$

$$q(\mathbf{r},s+\Delta s)\cong\exp\left[\frac{-\Delta s w(\mathbf{r})}{2}\right]q^{**}(\mathbf{r}) \qquad (23)$$

At this time, the intermediate step needs a calculation of the exponential function of the differential operator, and instead of performing this differential directly, performing Fourier transformation before the intermediate step and inverse Fourier transformation after the step and transposing the differential

operator to a simple multiplying operation are the core of this methodology.

The operation count necessary for this method is known as $O(MN\log M)$, which, in reality, is greatly affected by the optimization of Fast Fourier Transform (FFT).

III. Theoretical study on the nanostructure evolution of the diblock copolymer thin films in solvents

3.1. Introduction

Self-assembly of diblock copolymer has been studied by many researchers experimentally and theoretically. Specially, in area of semiconductor materials, photo lithography can adjust easily to making nanostructure pattern of thin film. Recently, many problems of semiconductor process are to solve development of processing and to reduce money practically. One of the semiconductor processes used recently is top-down method of photolessgrapy process which has many benefit of adjust for nowadays technology. But, they have a basic limits which are light distribution and wave of optical source, it is impossible to have a structure under 30 nm process. To overcome the problems mentioned above, current bottom-up process has getting attention.[35-42] Especially, block copolymer nanostructure is one of the cutting edge candidates to create a long range ordered microstructure. In the method of self-assembly lithography with BCPs, the most important point is how to control the defects in the way of microstructure evolution. In general experimental effort to make well-aligned block copolymer thin film structures, there are two main ways; solvent annealing and thermal annealing. Comparing those two methods, thermal annealing provides short-range ordered nanostructures and demands long time annealing. On the other hands, solvent evaporation and annealing is one of the most common methods to relatively easily and quickly create the block copolymer structure in thin films and enhance its long range ordered alignment in large area.[43] Also, it can be applicable to wide range of BCPs and there are less demands for pre-treatment of the substrates or BCP in this method than other methods. In spite of that, SCFT method which directly models solvent annealing system is not well established yet because of two reasons as followed.

i) Original SCFT formulas should be modified to account solvent effect to modeling solvent system. Thermodynamic parameters (e.g., volume fraction and χN) is hard to predict accurately because the microdomains of BCPs are dried and swollen as solvent evaporate.

ii) We should consider the way to deal with continuous time evolving process in modeling the experiment of solvent evaporation process.

In this chapter, I theoretical study on the nanostructure evolution on the diblock copolymer thin films in solvent annealing by using modified SCFT method for solvent system

3.2. Simulation Method

In this chapter, to simulate the mechanism of solvent evaporation process, solvent should be treated as C short homopolymers composed of C-type monomers. This way of modeling is distinguished from the original diblock copolymer SCFT dealing with only two domains, A and B, without any solvent. By considering the size ratio of polymer and solvent used in the actual experiment, the volume fraction of C short polymer in this simulation is set to be 5% of AB diblock copolymers. I investigated cylindrical and lamellar domain by setting A block fraction f of AB diblock copolymer as 0.3 and 0.5 respectively.

The starting points of formulas in this simulation method are modified diffusion equations (1) and (2) same as original SCFT calculation. The distinction between original SCFT and solvent system SCFT calculation, on the other hand, comes from C short polymer terms. So, the field equations and density functions should be modified to account them. To explain more details about this modified SCFT calculation, let me introduce four steps of this process briefly.

① Firstly, partial partition functions of AB diblock copolymers are obtained from the modified diffusion equations (1) and (2). The initial condition of the field energy is randomly generated by random number between 0 and 1.

② From the partial partition functions, the density functions of each blocks can be obtained by equation (6) and (7) in the same way of original SCFT. Here, we can calculate the density of C type short polymers (solvents) using Boltzmann factor as following equation (24), where $\phi_C(\mathbf{r})$ is the density of the solvent , V_C is volume of solvent and $w_C(\mathbf{r})$ is field potential acting on the solvent whose entire monomers are situated at point $\mathbf{r}$.

$$\phi_C(\mathbf{r}) = e^{-w_C(\mathbf{r})} V_C / \int d\vec{r} e^{-w_C(\mathbf{r})} \qquad (24)$$

③ Those three field energies of A, B and C parts of polymers can be obtained from modified field energy equation with density functions calculated at previous step. Field energy

equations are modified by adding C short polymer terms to apply contact energy of monomers of C short polymer (solvent).

$$w_A(\mathbf{r}) = \chi_{AB}N\phi_B(\mathbf{r}) + \chi_{CA}N\phi_C(\mathbf{r}) + \xi(\mathbf{r}) \qquad (25)$$

$$w_B(\mathbf{r}) = \chi_{AB}N\phi_A(\mathbf{r}) + \chi_{BC}N\phi_C(\mathbf{r}) + \xi(\mathbf{r}) \qquad (26)$$

$$w_C(\mathbf{r}) = \chi_{BC}N\phi_B(\mathbf{r}) + \chi_{CA}N\phi_A(\mathbf{r}) + \xi(\mathbf{r}) \qquad (27)$$

④ The newly obtained field energies calculated from the previous step is compared with the randomly chosen input field in the first step. If there are some differences between those two field energies, new input field of next cycle is determined by mixing old field and new field in 9:1 ratio. And then, ratio is redetermined by convergence test in the way that ratio of old field is increased in 1 % for positive convergence or deceased in 30 % for negative convergence. By using this newly obtained input field energy, we can continue another iterative simulation cycle by going back to stage 1.

In the case of non-solvent system, BCPs alignment mainly depends on heat and time, so it is hard to make defect-free pattern due to entropic fluctuation. By the way, in case of solvent annealing system, it is observed that the solvent density is higher at the site of the domain defects. As the annealing proceeds, the solvent fluidizes into the defects, and the defects are locally in the disordered regime. Since such solvent evaporation is continuous processes, it is impossible to carry out digitalized SCFT calculation with analog data. In order to track morphological change of block copolymer over time, I fix the amount of solvent, and then, find morphology of block copolymer corresponding to that solvent. As thickness of the film h and solvent volume fraction ψ decrease during solvent evaporation process, I model the quasi-static morphology evolution by using morphology of the thicker film as an input for the thinner film.

$$h = h_{dry} / (1-\psi) = h_{dry} / f_{ab} \qquad (28)$$

where h_{dry} is thickness of dry block copolymers film and f_{ab} is global volume fraction of polymers approaching to 1 as solvent evaporates. And, using random function, I introduce a small noise field to create the initial morphology. This method allows us to track down the detailed mechanism of the defect elimination. In this simulation, one of important parameters is χN_{eff} (effective χN). Since

solvent reduce the interaction strength between blocks of polymer chains, the effective value of χN is much lower than real χN value. Hence, I should introduce χN_{eff} parameter which is defined as following.

$$\chi N_{\text{eff}} = \chi N f_{ab} \qquad (29)$$

That parameter becomes important at onset of order-disorder transition and where the domain alignment is greatly enhanced during evaporation. Since fraction of diblock copolymer f_{ab} is always less than 1, χN_{eff} is always less than real χN. After phase transformation, nanostructures of BCPs are trapped by stable state where free energy is the minimum.

Lamellar domain and cylindrical domain has different solvent density range at which phase transition occurs and domain alignment is greatly enhanced. BCP phase diagram (figure 1b) tells the theoretically predicted χN_{eff} range (solvent density range) at each fractions of BCPs in system. In this study, I set $\chi_{AB}N = 25$, $\chi_{AC}N = 12$, $\chi_{BC}N = 10$ to represent well segregated microdomain for both cases of lamellar and cylindrical domain.

In this way, simulation cycle consists of four steps, to improve the speed of calculations, I carry out some part of calculation in parallel. Parallel computing is applied to solve tridiagonal matrix equation (13), (14), and (15). Parallel processing is realized in environment of Linux using UNIST HPC (High Performance Computer). Intel Xeon X5650 (2.66GHz, 16cores/machine) processor is used and heterogeneous computing is carried out by OpenMPI library. In real calculation for 128x128x32 grid simulation box, parallized system with 16cores improves calculation efficiency by 12 times with 2.8 s, comparing 35 s to operate l iteration calculation.

3.3. Results and Discussion

According to the BCPs phase diagram (figure 1b), it is predicted that disordered-lamella phase transition occurs at $\chi N_{\text{eff}} = 10.5$ for the case of lamellar domain ($f = 0.5$). When block fraction of BCPs is 0.3 (cylindrical domain), cylindrical domain has disordered-spherical phase transition at

which χN_{eff} is equal to 15. From the χN_{eff} equation (29), I can calculate those phase transition solvent density as 55% for lamellar domain ($f = 0.5$) and as 41% for cylindrical domain ($f = 0.3$)
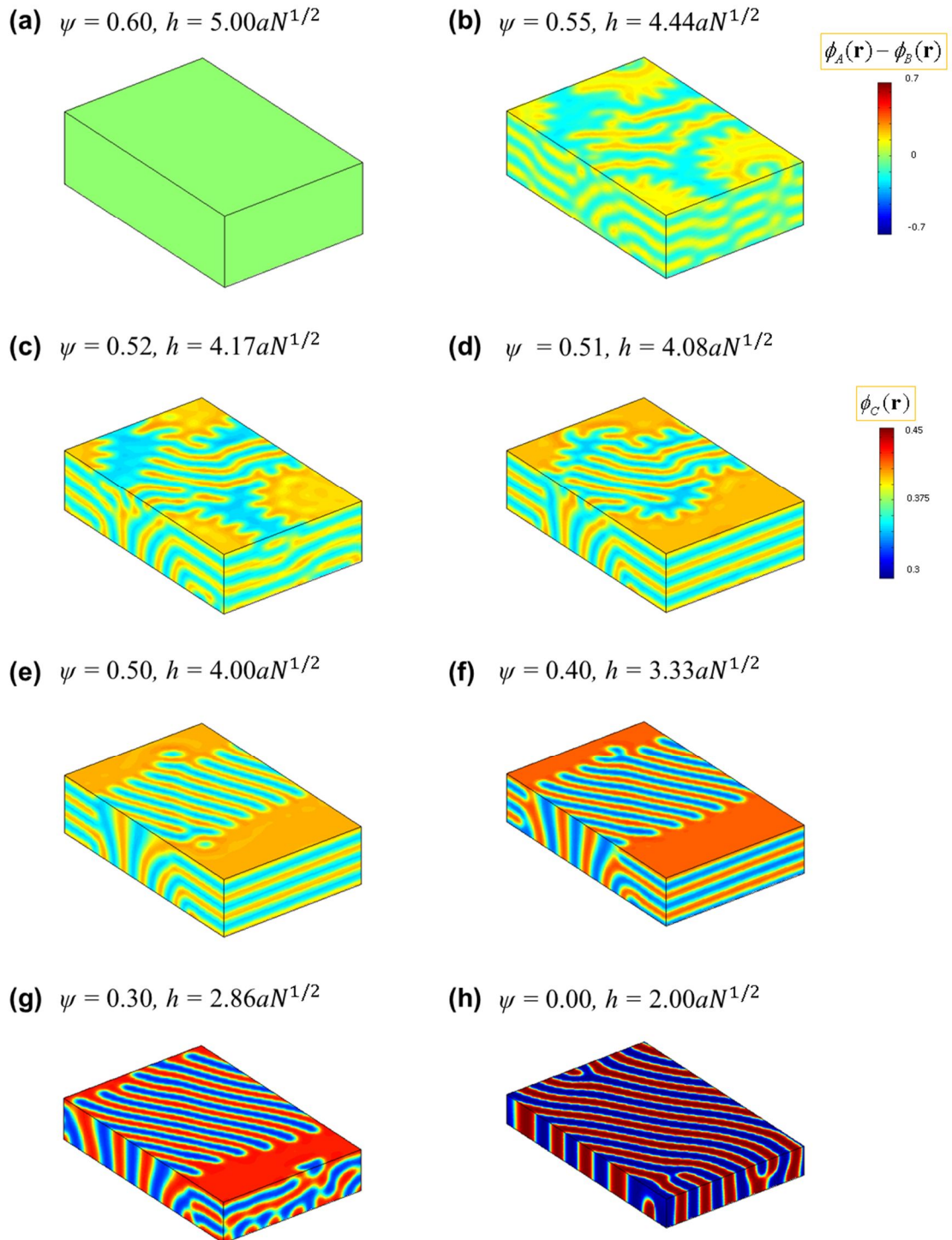
In this simulation, considering real thin film system, I set size of *x*-axis and *y*-axis as 16, 10.39 respectively (the unit length is set to be $a^2 N = 1$). To simulate the situation of thickness decreasing during solvent evaporation, I make size of *z*-axis (height) to decrease linearly as 4 at 50% of solvent and 2 at 0%. To simulate time evolving pattern of phase transition, I model the quasi-static morphology evolution with input-output program. The boundary conditions used in this calculation are periodic boundary for *x* and *y* axis and reflecting boundary for *z* axis.

3.3.1. Lamellar Domain ($f = 0.5$)

From phase diagram (figure 1b) and equation (29) of χN_{eff}, phase transition is predicted to occur at 55% of solvent. The color represents density difference between A and B segments of polymers. As solvents evaporate, height of film *h* decreases and disordered pattern transit to ordered lamellar pattern with horizontal lamella and vertical lamellar pattern mixed at 51% of solvent (slightly different from theoretically predicted value 55%). Horizontal lamellae are observed at initial stage of phase transformation, but as solvent evaporation proceeds, vertical lamellae are more observed. The reason of that is considered to be commensurability of periodic length of lamellar domain and thickness of film. To form lamellar pattern, system should have commensurable periodic length of lamellar domain along with axis size, or system size should be large enough to cancel out energy penalty from mismatch.[44] For the relatively high solvent % case, height of system is large enough to cancel out energy penalty from mismatch, so both horizontal lamellae and vertical lamellae can exist simultaneously. As solvent evaporate more and more, on the other hand, the height of thin films more decreased continuously, so quantization requirement of system size for vertical lamellae become harder to satisfy.

It is concluded that vertical lamellae are more preferred than horizontal lamellae at low % of solvent. As evaporation proceeds, the domain alignment is greatly enhanced, and well aligned vertical lamellae are finally observed.

It is confirmed that, from the Figure 4a-h, solvent annealing not only affect the speed of pattern alignment but also help defects eliminated. It is predicted to be helpful that directed self-assembly method[45] can be used together with solvent annealing method to get more effectively domain aligned system.

(a) $\psi = 0.60$, $h = 5.00aN^{1/2}$

(b) $\psi = 0.55$, $h = 4.44aN^{1/2}$

$\phi_A(\mathbf{r}) - \phi_B(\mathbf{r})$

0.7

0

-0.7

(c) $\psi = 0.52$, $h = 4.17aN^{1/2}$

(d) $\psi = 0.51$, $h = 4.08aN^{1/2}$

$\phi_C(\mathbf{r})$

0.45

0.375

0.3

(e) $\psi = 0.50$, $h = 4.00aN^{1/2}$

(f) $\psi = 0.40$, $h = 3.33aN^{1/2}$

(g) $\psi = 0.30$, $h = 2.86aN^{1/2}$

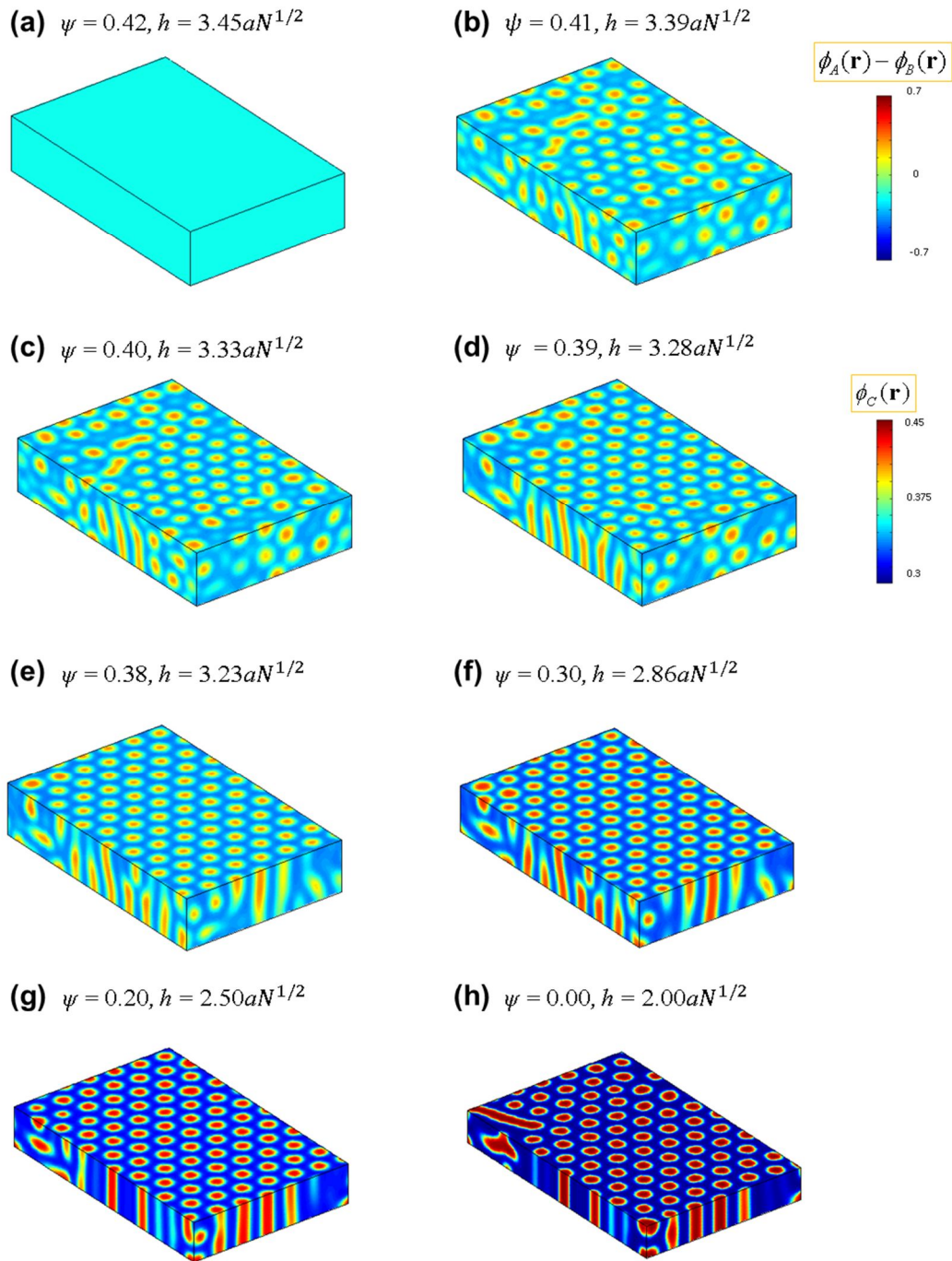**(h)** $\psi = 0.00$, $h = 2.00aN^{1/2}$

Figure 4. Simulation results of *AB* block copolymer thin films in solvents for lamellar domain. The thickness of films *h* changes according to the solvent density ψ. The domain alignment is greatly

enhanced as evaporation proceeds (Disordered State → Horizontal and Vertical Lamellae → Vertical Lamellae → Well-aligned Vertical Lemellae).

3.3.2. Cylindrical Domain ($f = 0.3$)

Unlike lamellar domain, in cylindrical domain case, there are two phase transition during the evolution of nanostructure of *AB* block copolymers. As known from *AB* block copolymer phase diagram, in nonsolvent system, disordered-spherical phase transition occurs at which χN_{eff} is equal to 14, and spherical-cylindrical phase transition occurs at which χN_{eff} is equal to 15. For solvent system, considering equation (29) of χN_{eff} with $\chi_{AB} N = 25$, disordered-spherical phase transition is predicted to occurs at 44% of solvent and spherical-cylindrical phase transition is predicted to occurs at 40% of solvent.

In the actually conducted simulation, the results were slightly different from the theoretical values obtained from phase diagram. It was observed that disordered-spherical phase transition occurs at 41% of solvent and spherical-cylindrical phase transition occurs at 39% of solvent (See, Figure 5a-h). The reason is considered to be that at disordered-spherical phase transition point, high solvent density reduces interaction strength between two blocks, which results in mixed state with randomly disordered pattern and spherical pattern. At spherical-cylindrical phase transition point, solvent density is of little importance to influence high interaction strength χN , so two blocks separate greatly to form cylindrical pattern. As shown from the Figure 5a-h, vertical cylinder pattern is almost dominantly preferred than horizontal one. The reason why that happens is similar with lamellar case. It is harder to satisfy quantization requirement to form horizontal cylindrical pattern than vertical cylindrical one in continuously changing thickness of the system. As solvent evaporation proceeds, free energy dramatically decreased to give out hexagonal patterns. These simulation results also show that solvent annealing is very effective method to enhance cylindrical domain alignment in short time with low defects.

(a) $\psi = 0.42, h = 3.45aN^{1/2}$

(b) $\psi = 0.41, h = 3.39aN^{1/2}$

$\phi_A(\mathbf{r}) - \phi_B(\mathbf{r})$

(c) $\psi = 0.40, h = 3.33aN^{1/2}$

(d) $\psi = 0.39, h = 3.28aN^{1/2}$

$\phi_C(\mathbf{r})$

(e) $\psi = 0.38, h = 3.23aN^{1/2}$

(f) $\psi = 0.30, h = 2.86aN^{1/2}$

(g) $\psi = 0.20, h = 2.50aN^{1/2}$

(h) $\psi = 0.00, h = 2.00aN^{1/2}$

Figure 5. Simulation results of *AB* block copolymer thin films in solvents for cylindrical domain. The thickness of films h changes according to the solvent density ψ. The domain alignment is greatly enhanced as evaporation proceeds (Disordered State → Spheres → Cylinders → Cylinders with Less Defects).

IV. Arrangement of Microdomains of Diblock Copolymer Confined in Half-Ellipsoid-Shape Confinements Having Two Controlled Interfaces

4.1. Introduction

Confinement of the diblock copolymers under certain geometries can offer new methods to develop unique morphologies which have never been known before in bulk or thin film.[46-49] For example, symmetric diblock copolymer usually shows lamellar arrangement in bulk state. On the other hand, recent experimental results report that new interesting onion-shape lamellar morphologies were observed in a half sphere shape confinement. In this chapter IV, I theoretically study various block copolymer morphologies in hemispherical and ellipsoidal shape nanobowl confinements and compare the results with experiments.

The key parameters for the morphology determination in ellipsoidal confinement are the size and shape of the container and the surface tension between surface of confining geometry and each block components of polymers. For example, commensurability between the lamellar domain spacing L_0 in bulk and the diameter D of the nanobowl container is one of the most important parameters to control lamellar morphology in the confinement. Additionally, depending on the eccentricity of the ellipsoid, the curvature of the spherical geometry influences the lamellar morphology for ellipsoidal confinements. Most of all, affinity between surface of confining geometry and block copolymer is the most important parameters to control the morphologies. The degree of commensurability did not affect much the arrangement of the lamellae compared with the surface selectivity at the cavity wall.

Our theoretical modeling uses self-consistent field theory (SCFT) which calculates the mean field density distribution of segments of *AB* block copolymers in this confined geometry. Predictions based on the SCFT calculation were compared with the morphologies obtained in experiment and found that they are reasonably consistent.

In the experiment, polystyrene-*block*-poly(methyl methacrylate) copolymer (PS-*b*-PMMA) are physically confined in half spherical anodic aluminum oxide nanobowl, and their morphology is controlled by the top cover polymer film and the cavity surface, which may interact selectively

depending on the coating of the nanobowl.[50] Three different types of surface interaction are prepared by grafting the nanobowl wall with three different brushes. PMMA-OH and PS-OH brushes work as selective surfaces, and PS-*ran*-PMMA copolymer brush work as a neutral brush. Selectivity of the top surface of the cavity can also be controlled by covering three different kinds of films such as PMMA homopolymers, PS homopolymers, and PS-*ran*-PMMA copolymers. When these two interfaces are controlled independently, the alignment of BCP microdomains can be significantly changed and thus new kinds of morphology were observed. In this study with SCFT method, I model, polystyrene-*block*-poly(methyl methacrylate) copolymer (PS-*b*-PMMA) as *AB* block copolymers (*A* and *B* corresponds to PMMA and PS, respectively).

In this chapter, I investigate arrangement of not only lamellar domain (symmetric diblock copolymer domain) but also cylindrical domain and spherical domain (asymmetric diblock copolymer domain) by changing parameter *f* (*A* fraction of *AB* diblock copolymer). In the case of spherical domain, very interesting ring structure was observed. Also, effect of the curvature of the ellipsoidal geometry is investigated to figure out how the eccentricity of ellipsoid affects block copolymer morphologies in ellipsoidal shape nanobowl confinements.

4.2. Theory and Numerical Implementation

The alignment of microdomains of *AB* block copolymer with a volume fraction of *A* block having *f* was calculated by the SCFT method with some modifications given below. In this study, I set $\chi_{AB}N = 35$ to represent well segregated microdomains in a hemispherical cavity.

To describe the preference of the top surface layer to each block component, I introduced two new parameters, and η_B. The top surface property in the theoretical model is controlled by imposing delta function-like surface interaction, and the two parameters, η_A or η_B, represent the delta function strength. The sign of the parameters is chosen such that if η_A is positive, there exists favorable interaction of the cover film to *A* component. To exclude the BCP chains from the outside of the cavity, *C* homopolymer with the same segment number *N* and statistical segment length *a* is introduced. Outside of the cavity, *C* homopolymer is fixed by $w^{\text{external}}(\mathbf{r}) = 30$ in the following self-

consistency equations (30-32).

$$w_A(\mathbf{r}) = -2\eta_A \delta(z)aN^{1/2} + \chi_{AB}N\phi_B(\mathbf{r}) + \chi_{AC}N\phi_C(\mathbf{r}) + \xi(\mathbf{r}) \qquad (30)$$

$$w_B(\mathbf{r}) = -2\eta_B \delta(z)aN^{1/2} + \chi_{AB}N\phi_A(\mathbf{r}) + \chi_{BC}N\phi_C(\mathbf{r}) + \xi(\mathbf{r}) \qquad (31)$$

$$w_C(\mathbf{r}) = \chi_{AC}N\phi_A(\mathbf{r}) + \chi_{BC}N\phi_C(\mathbf{r}) + \xi(\mathbf{r}) + w^{\text{external}}(\mathbf{r}) \qquad (32)$$

where $\phi_i(\mathbf{r})$ is the segment density of i type polymers, $\xi(\mathbf{r})$ is the pressure field, and $w_i(\mathbf{r})$ is the field acting on them. As mentioned above, the preference of the top surface to each type of material was assigned by setting either η_A or η_B parameter as 0.4.

The simulation box consisted of a 3-dimensional 64x64x64 grid, and the modified diffusion equations for the partition functions of block copolymers and homopolymers were solved using the SCFT with pseudospectral method modified for this research.[51-52] For both block copolymers and a homopolymer, 50 mesh points were used in the polymer length direction. The Neumann boundary condition was used for all boundaries to correctly represent the polymer/film, interface, while minimizing the unit cell size.

4.3. Results and Discussion

4.3.1. Symmetric Diblock Copolymer (Lamellar Domain f = 0.5)

Figure 4 summarizes the result by showing the morphology behavior at a few given parameter values. The most important parameter determining the block copolymer morphology is flory-huggins parameter χ between polymer segments, and surface interaction parameter η. In this study, I set $\chi_{AB}N = 35$ to represent well segregated lamellar domains in a hemispherical cavity with a size $D = 4.0L_0$. When these parameters are used, the domain spacing L_0 of lamellar phases in the bulk is given by $L_0 = 1.95aN^{1/2}$.

Because the boundary of the system is spherically symmetric, I will show the morphologies using

vertical cross section of the system from now on. In the figure, the red and blue colors represent A (PMMA) and B (PS) blocks, respectively. For better visualization, the C homopolymer filled vessel that determines the hemispherical cavity shape is shown in green.
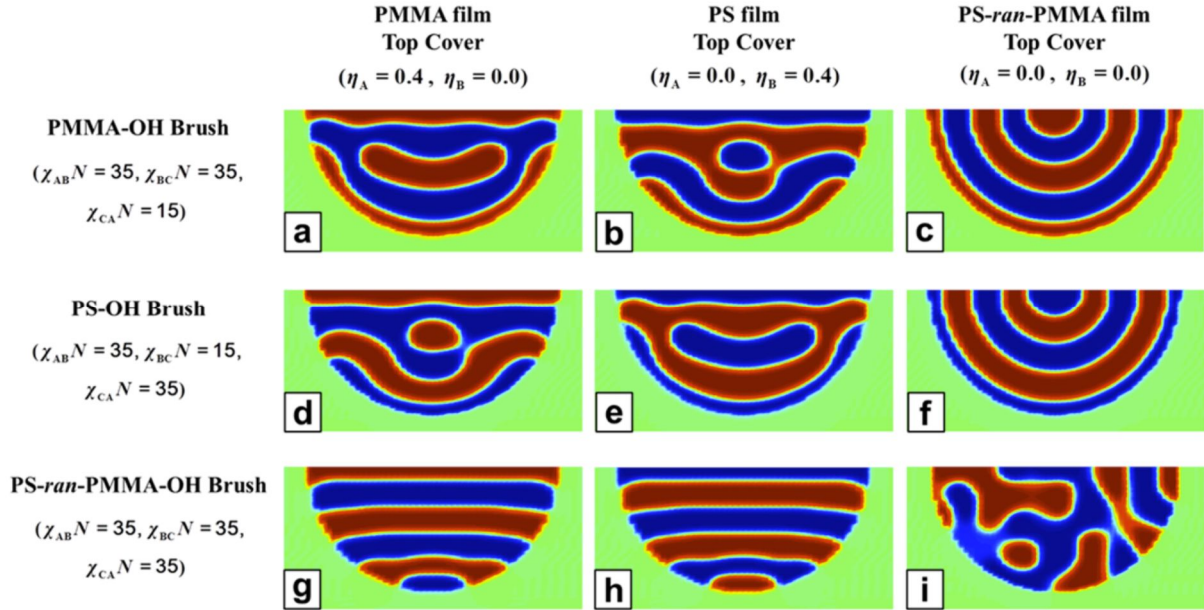

Figure 6. Microdomain alignments of AB block copolymer (PS-b-PMMA) confined within a hemispherical cavity calculated by SCFT pseudospectral method. The polymer-grafted cavity walls are modeled as C homopolymers (green color). By controlling their interaction with A and B segments, the walls are covered by three different polymer brushes: PMMA-OH (top panel), PS-OH (middle panel), and PS-ran-PMMA-OH (bottom panel). Also, the top surface preference is given as a delta function-like potential with η_A and η_B, representing the delta function strength. The red and blue colors represent A (PMMA) and B (PS) blocks, respectively.

When the cavity is covered by PMMA-OH brush, I set $\chi_{CA}N = 15$ and $\chi_{BC}N = 35$ to represent the preference of cavity wall for PMMA. In this case, the arrangement of lamellae highly depends on the top surface interaction (Figures 6a-6c). If the top surface prefers one type of segment (Figures 6a and 6b), a parallel lamellar structure is observed on the top surface due to the preferential surface interaction, and concentric lamellae are observed at the bottom of the cavity due to the inner wall brush which prefers one type of segment. The combined structure of parallel lamellae and concentric

lamellae is consistent with experimental results. On the other hand, when the top layer becomes neutral, concentric lamellae with outermost PMMA shell is observed until they meet the top layer, as shown in Figure 6c.

When the cavity is covered by PS-OH brush, I set $\chi_{C_A}N = 35$ and $\chi_{BC}N = 15$, and the observed morphologies are very similar to those in the cavity covered by PMMA-OH, except that the outmost cavity wall is PS layer (Figures 6d-6f). One can easily check that Figures 6a and 6e are essentially the same except for the coloring, and the same relation holds true for Figures 6b and 6d, and Figures 6c and 6f.

The most interesting case is when the cavity wall is covered by PS-*ran*-PMMA-OH brush. To represent this case, I set $\chi_{C_A}N = 35$ and $\chi_{BC}N = 35$, and the results are shown in Figures 6g-6i. When the top surface has a preference for one type of segment, staked lamellae are observed (Figures 6g and 6h), while bi-continuous structures having interconnected lateral and vertical lamellae are observed for a neutral top layer (Figure 6i). The formation of bi-continuous morphology could be explained as follows. The cavity has a bowl shape, and it is obvious that the lamellae must be distorted at the bottom parts of the cavity even if they are perpendicular to the upper surface. The distortion of lamellae imposes additional entropic penalty, which may provide driving force towards bi-continuous domain formation. The morphology as shown in Figure 6i was obtained by using random fields as an input. In SCFT methodology, it is practically impossible to prove if such a morphology is in a true equilibrium, but I used many other inputs to create competing morphologies and found this one most favorable. Thus, it is highly plausible that the bi-continuous morphology is at least very close to the free energy minimum, and it is not surprising that experiments *did* find a similar morphology. For a better visualization of the bi-continuous morphology, its 3D structure is demonstrated in Figure 7. Our simulation results show that only morphologies whose *AB* boundary is perpendicular to the top surface can survive when the top surface is not preferential.
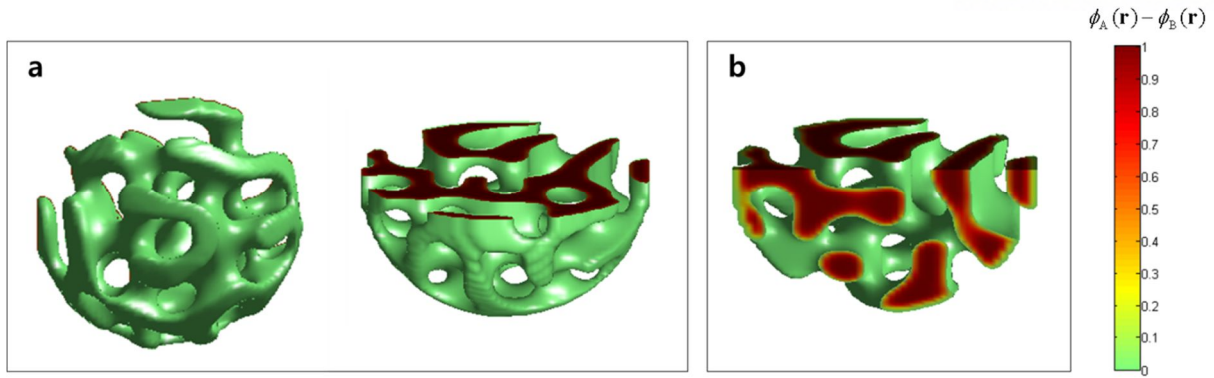
Figure 7. (a) 3 dimensional visualization of the bi-continuous morphology corresponding to Figure 6i after slicing the sample at two different angles (bottom view (left) and lateral (right) view). For better visualization, only PS microdomains are deleted. (b) Cross-sectional image of Figure 7a. The cutting angle is chosen so that the cross section is virtually the same as Figure 6i.

4.3.2. Asymmetric Diblock Copolymer (Cylindrical Domain $f = 0.25$)

In this section, I investigate asymmetric diblock copolymer arrangement in hemispherical confinement with cylindrical domain (A block fraction $f = 0.25$). Again, $\chi_{AB}N$ is set to be 35 to represent well segregated cylindrical microdomains and diameter D of a hemispherical cavity is also equal to $4.0L_0$, where L_0 in this section represents period of cylindrical domain in bulk state. Generally, asymmetric diblock copolymer with these parameters (block fraction $f = 0.25$ and $\chi_{AB}N = 35$) without any confinement shows vertical or horizontal cylinder structure as shown in chapter 3, or mixed one in bulk state. In the spherically confined structure, however, with help of interactions with two controlling interfaces, spherically symmetric ring structures lying horizontally around the wall of nanobowls were observed. The Figure 8 shows the effects of three different cover film interactions on the confined morphologies assorted by three columns; PMMA film top cover (first column), PS film top cover (second column), and PS-*ran*-PMMA film top cover (third column). Each row represents selective brushes (PMMA-OH brush used) and random brush case, respectively.
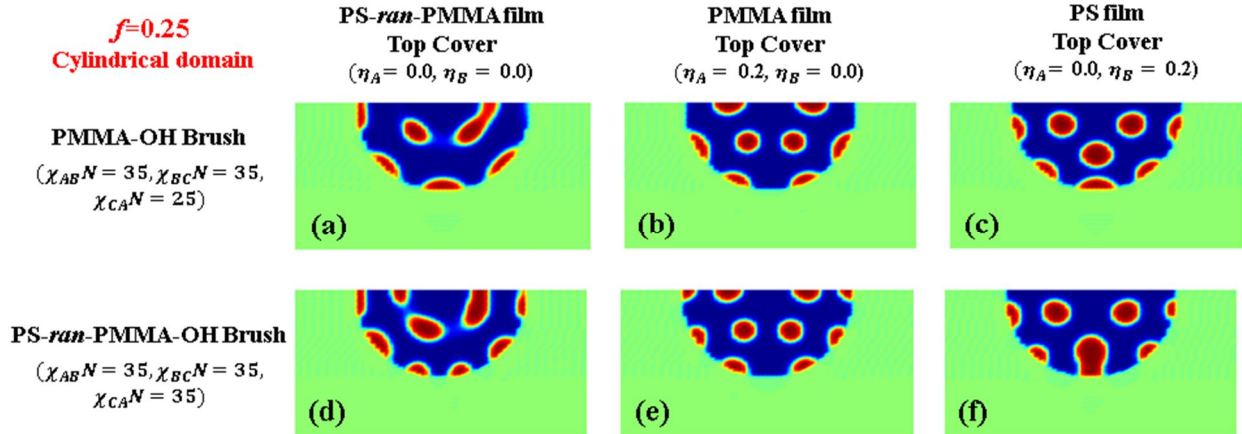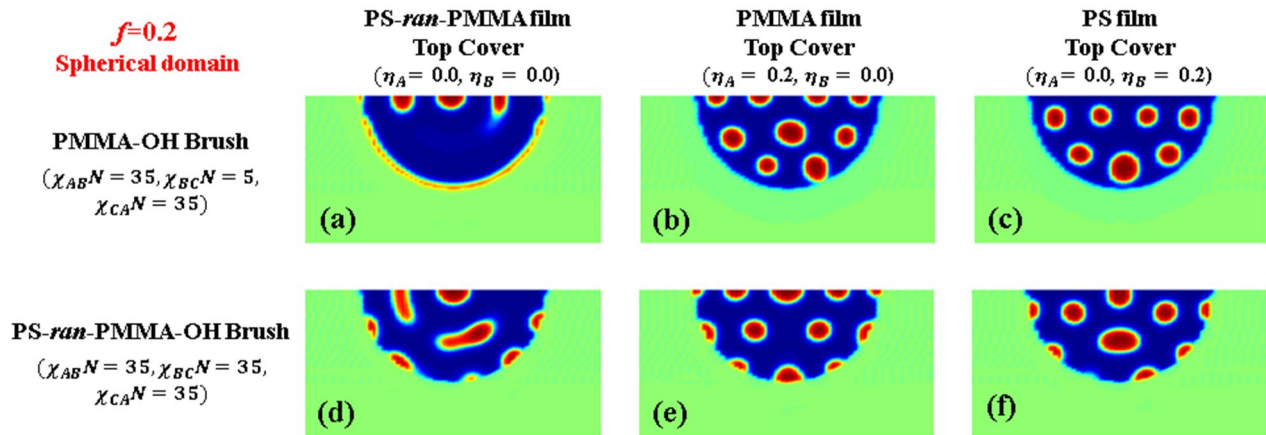
Figure 8. Microdomain alignments of asymmetric *AB* block copolymer (PS-*b*-PMMA) confined within a hemispherical cavity calculated by SCFT pseudospectral method for cylindrical domain.

If wall of nanobowl container is coated with PMMA-OH brush ($\chi_{CA}N = 25$), outmost ring structure of A block domain is formed along the wall of the container with help of attractive wall interaction by *A*-selective brush. Depending on the three cover film, each cases shows slightly different alignment. If random cover film is used, well arranged structure is shown close to the wall interface, but toward the inside of container, structure becomes distorted due to less driving force of orientation. It is considered to be that there must be two selective interfaces which drive to form well-aligned ring structure of cylindrical domain to the inside of nanobowl confinement (Figure 8b and 8c). It is proved by Figure 8b and 8c, at which PMMA film covering and PS film covering is acted as driving force for alignment of morphology respectively. If PS-*r*-PMMA-OH brush is used ($\chi_{CA}N = 35$) for the coating of the nanobowl wall, very similar results but less ordered structures (Figure 8d-f) were obtained as the cases of selective PMMA-OH brush one. However, for the random brush and random cover are used, similar with Figure 8a, but more disordered structure was observed due to less driving force of orientation.

### 4.3.3. Asymmetric Diblock Copolymer (Spherical Domain *f* = 0.2)

In this section, I investigate asymmetric diblock copolymer arrangement in hemispherical confinement with spherical domain (A block fraction *f* = 0.2). Again, $\chi_{AB}N$ is equal to 35 and diameter

D of a hemispherical cavity is set to be equal to $6.0L_0$, where L_0 in this section represents period of spherical domain in bulk state. Even though we expect spherical morphology as in bulk state, simulation results for the arrangement of asymmetric diblock copolymers with $f = 0.2$ in nanobowl container shows very similar morphologies with cylindrical domain case. The results are shown as following Figure 9. The roles of each controlling surfaces (top cover film interface and interface with wall of container) are very similar with cylindrical domain case. Again, it is confirmed that two selective interfaces are required to make well-aligned nanostructures of AB block copolymers.

Figure 9. Microdomain alignments of asymmetric AB block copolymer (PS-b-PMMA) confined within a hemispherical cavity calculated by SCFT pseudospectral method for spherical domain.

4.3.4. Effects of the Curvature of the Ellipsoidal Geometry on Morphology of Symmetric Diblock Copolyme
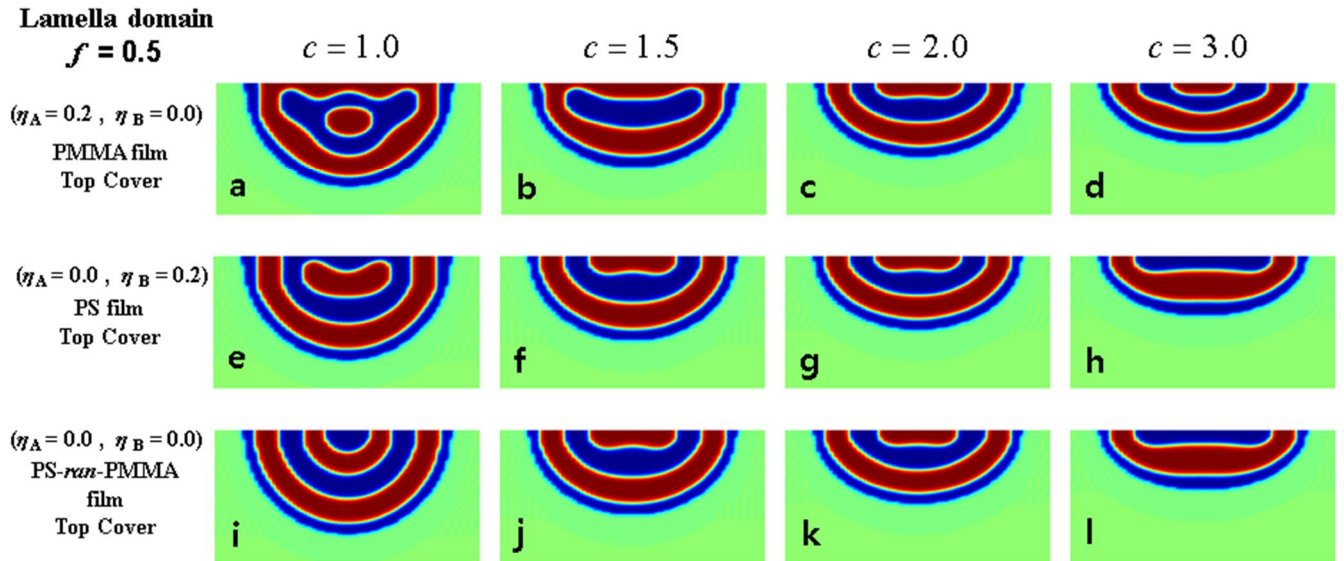
Figure 10. Vertical cross-sectional simulation images of microdomain structures of PS-*b*-PMMA confined at ellipsoidal cavities with different depth.

I also investigate the dependence of ellipsoidal cavities depth on BCP alignment at constant $\chi_{ij}N$ parameters (for all the Figures, $\chi_{AB}N = 35$, $\chi_{BC}N = 25$, $\chi_{CA}N = 35$) with lamellar domain ($f = 0.5$). Each column represents different depth of nanobowls and each row represent three different applications of top cover films. The shapes of the bowls were represented by the equation $x^2 + y^2 + cz^2 = D^2$, and I control the depth of cavities by changing the parameter c in the equation. As the depth of confinement becomes narrower, much less spherical layers are contained inside and isolated sphere becomes disappear. It is concluded that by changing the depth of the nanobowls, the number of layers in the cavities can be controllable.

V. Conclusion

The main content of this thesis is about the theoretical study on arrangement of microdomains of diblock copolymer in solvent vaporization (Chapter III) and in hemi-spherically confined system (Chapter IV). The theoretical tool in this research is SCFT which has been on major tool investigating block copolymer structure for past two decades. In the simulation of block copolymer thin films in solvent annealing process, I used the morphology of the thicker film as an input for the thinner film to model the quasi-static morphology evolution. As the solvents evaporate, it is found that the thickness of the film h decreased and the number of defects reduced producing well-aligned domain structure. For the cylindrical case, vertical domains are preferred during the evaporation process rather than horizontal domain. The onset of order-disorder transition is found near the theoretical prediction. This method allows us to track down the detailed mechanism of the defect elimination and remind fact that domain alignment is greatly enhanced as evaporation proceeds. I also investigated the microdomain structures of polystyrene-*block*-poly(methyl methacrylate) copolymer (PS-*b*-PMMA) confined at hemispherical cavities having two controlling interfaces, top cover layer and inner cavity wall. Confinement of the diblock copolymers under ellipsoidal geometries offer new methods to develop unique morphologies which have never been known before in bulk or thin film. For example, when the container wall is coated with PS polymers and neutral cover film is used, onion-shape lamellar phases with PS at the bottom is observed rather than the parallel lamellar phases. It is also found that preferential cover film-polymer surface interaction promotes the alignment of domains. The most interesting case is when the cavity wall is covered by PS-*ran*-PMMA-OH brush and a neutral top layer is used on the nanobowl container. The very interesting bi-continuous structures having interconnected lateral and vertical lamellae are observed (Figure 6i). These novel morphologies found in this study could be used as surface enhanced Raman scattering (SERS), Fano resonance and anisotropic optical properties, because the hemispherical shape would provide broken symmetry to generate plasmon hybridization, which could not be obtained by fully spherical shape.

REFERENCES

[1] Lazzari, M., Liu, G., Lecommandoux, S., Eds. *Block Copolymers in Nanoscience*; Wiley-VCH: Weinheim, 2006.

[2] Klok, H. A.; Lecommandoux, S. *Advanced Materials*. **2001**, *13*, 1217-1229.

[3] O'Reilly, R. k.; Hawker, C. J.; Wooley, K. L. *Chemical Society Review*. **2006**, *35*, 1068-1083.

[4] Black, C. T. *nature Nanotechnology*. **2007**, *2*, 464-465.

[5] Bates, F. S. and Fredrickson, G. h. "Block Copolymer Thermodynamics - Theory and Experiment"*, Annu. Rev. Phys. Chem*.**1990**, *41*, 525-557 .

[6] R. J. Spontak, R. Shankar, M. K. Bowman, A. S. Krishnan, M. W. Hamersky, J. Samseth, M. R. Bockstaller and K. O. Rasmussen. *Nano Letters*. **2006**, *6*, 2115-2120.

[7] J. Masuda, A. Takano, Y. Nagata, A. Noro, and Y. Matsushita. *Physics Review Letters*. **2006**, *97*, 098301.

[8] S. M. Park, G. S. W. Craig, C. C. Liu, Y. H. La, N. J. Ferrier, and P. F. Nealey. *Macromolecules*. **2008**, *41*, 9118-9123.

[9] Cheng, J. Y., Ross, C. A., Chan, V. Z.-H., Thomas, E. L., Lammertink, R. G. H. and Vancso, G. J. "Formation of a Cobalt Magnetic Dot Array via Block Copolymer Lithography"*, Adv. Mater.* **2001**, *13*, 1174-1178.

[10] Thurn-Albrecht, T., Schotter, J., Kastle, C. A., Emley, N., Shibauchi, T., Krusin-Elbaum, L., Guarini, K., Black, C. T., Tuominen, M. T. and Russell, T. P. "Ultrahigh-density Nanowire Arrays Grown in Self-assembled Diblock Copolymer Templates", *Science*. **2000**, *290*, 2126-2129.

[11] Lopes, W. A. and Jaeger, H. M., "Hierarchical Self-assembly of Metal Nanostructures on Diblock Copolymer Scaffolds", *Nature*.**2001**, *414*, 735-738.

[12] Park, M., Harrison, C., Chaikin, P. M., Register, R. A. and Adamson, D. H., "Block Copolymer Lithography : Periodic Arrays of ~1011 Holes in 1 Square Centimeter," *Science*. **1991**, *276*, 1401-1404.

[13] Li, P. R., Dapkus, P. D., Thompson, M. E., Jeong, W. G., Harrison, C., Chaikin, P. M., Register, R. A. and Adamson, D. H., "Dense Arrays of Ordered GaAs Nanostructures by Selective Area Growth

on Substrates Patterned by Block Copolymer Lithography," *Appl. Phys. Lett.*, **2000**, *76*, 1689-1691.

[14] Shin, K., Leach, K. A., Goldbach, J. T., Kim, D. H., Jho, J. Y., Tuominen, M., Hawker, C. J. and Russell, T. P., "A Simple Route to Metal Nanodots and Nanoporous Metal Films," *Nano Letters*, **2002**, *2*, 933-936.

[15] A. K. G. Tavakkoli, K. W. Gotrik, A. F. Hannon, A. Alexander-Katz, C. A. Ross and K. K. Berggren, *Science*, *336*, 1294-1298.

[16] W. A. Lopes and H. M. Jaeger. *Nature*. **2001,** *414*, 735-738.

[17] A. Balazs, T. Emrick and T. P. Russell. *Science*. **2006**, *314*, 1107-1110.

[18] M. Bockstaller, R. Kolb and E. L. Thomas. *Adv. Mater*. **2001**, *13*, 1783-1786.

[19] T. Thurn-Albrecht, J. Schotter, G. A. Kastle, N. Emley, T. Shibauchi, L. Krusin-Elbaum, K. Guarini, C. T. Black, M. T. Tuominen and T. P. Russell. *Science*. **2000**, *290*, 2126-2129.

[20] F. Droplet and G. H. Fredrickson. *Phys. Rev. Lett*. **1999**, *83*, 4317-4320.

[21] J. U. Kim and M. W. Matsen. *Macromolecules*. **2008**, *41*, 246-252.

[22] J. U. Kim amd M. W. Matsen. *Phys. Rev. Lett*. **2009**, *102*, 078303.

[23] S. Jeong, H. Moon, J. Shin, B. Kim, D. Shin, J. Kim, Y. Lee, J. Kim and S. Kim, *Nano Letters*, *10*, 3500-3503

[24] J. U. Kim, Y. B. Yang and W. B. Lee. *Macromolecules*.**2012**, *45*, 3263-3269.

[25] M. W. Matsen and M. Schick. *Phys. Rev. Lett*. **1994**, *72*, 2660-2663.

[26] M. W. Matsen and F. S. Bates. *Macromolecules*.**1996**, *29*, 7641-7644.

[27] M. W. Matsen and F. S. Bates, J. *Chem. Phys*. **1997**, *106*, 2436-2448.

[28] K. O. Rasmussen and G. Kalosakas, J. Polym. *Sci. Part B-Polymer Physics*. **2002**, *40*, 1777-1783.

[29] E. W. Cochran, C. J. Garcia-Cervera, G. H. Fredrickso., *Macromolecules*. **2006**, *39*, 2449.

[30] A. Ranjan, J. Qin, D. C. Morse. *Macromolecules*. **2008**, *41*, 942.

[31] P. Stasiak and M. W. Matsen, Eur. *Phys*. **2011**, *J. E 34*, 110-118.

[32] W. H. Press, S. A. Teukolsky and W. T. Vetterling, Numerical Recipes in C: The Art of Scientific Computing, Cambridge University Press: Cambridge, U. K., 1993.

[33] K. O. Rasmussen and G. kalosakas, J. *Polym. Sci. Part B-Polymer Physics*. **2002**, *40*, 1777-1783.

[34] P. Stasiak and M. W. Matsen. *Eur. Phys. J. E.* **2011**, *34*, 110-118.

[35] C. J. Hawker and T P. Russell. *MRS*. Bull.**2005**, *30*, 952.

[36] M. J. Fasolka and A. M. Mayes, Ann. *Rev. Mater. Res.* **2001**, *31*, 323.

[37] C. T. Black, R. Ruiz, G. Breyta, J. Y. Cheng, M. E. Colburn, K. W. Guarini, H. C. Kim, and Y. Zhang, IBM J. *Res. Dev.* **2007**, *51*, 605.

[38] J. Y. Cheng, C. A. Ross, H. I. Smith, and E. L. Thomas. *Adv. Mater.* **2006**, *18*, 2505.

[39] J. K. Kim, J. I. Lee, and D. H. Lee, *Macromol. Res.* **2008**, *16*, 267.

[40] M. P. Stoykovich and P. F. Nealey. *Mater. Today.***2006**, *9*, 20.

[41] C. T. Black. *ACS Nano*. **2007**, *1*, 147.

[42] C. T. Black, Nat. *Nanotechnol*. **2007**, *2*, 464.

[43] KIM, Seung Hyun, et al. Highly oriented and ordered arrays from block copolymers via solvent evaporation. *Advanced Materials*. **2004**, *16.3*: 226-231.

[44] TAKAHASHI, Hassei, et al. Defectivity in laterally confined lamella-forming diblock copolymers: Thermodynamic and kinetic aspects. Macromolecules, **2012**, *45.15*: 6253-6265.

[45] HOONÁKIM, Bong; YOUNGÁKIM, Ju; OUKÁKIM, Sang. Directed self-assembly of block copolymers for universal nanopatterning. *Soft Matter*, **2013**.

[46] Stewart-Sloan, C. R.; Thomas, E. L. *Eur. Polym. J.* **2011**, *47*, 630-646.
[47] Shi, A. -C.; Li, B. *Soft Matt.* **2013**, *9*, 1398-1413.
[48] Yu, B.; Sun, P.; Chen, T.; Jin, Q.; Ding, D.; Li, B.; Shi, A. -C. *Phys. Rev. Lett.* **2006**, *96*, 138306.
[49] Xu, T.; Hawker, C. J.; Russell, T. P. *Macromolecules* **2001**, *34*, 3458-3470.
[50] Bae, D. S.; Jeon, G. H.; Jinnai, H.; Huh, J.; Kim, J. K. *Macromolecules* **2013**, *46*, 5301-5307.
[51] Rasmussen, K. O.; Kalosakas, G. *J. Polym. Sci., Part B: Polym. Phys.* **2002**, *40*, 1777-1783.
[52] Stasiak, P.; Matsen, M. W. *Eur. Phys. J. E.* **2011**, *34*, 110.
[53] Sarah Kim, Dong Ok Shin, Dae-Geun Choi, Jong-Ryul Jeong, Jeong Ho Mun, Yong-Biao

Yang, Jaeup U. Kim, Sang Ouk Kim, and Jun-Ho Jeong, Graphoepitaxy of Block Copolymer Self-Assembly Integrated with Single Step ZnO Nanoimprint", *Small* , **8**, 1563-1569.